Magnetoinductive polaritons: Hybrid modes of metamaterials with interelement coupling

E. Shamonina*

Optical and Semiconductor Devices Group, Electrical and Electronic Engineering (EEE) Department, Imperial College, Exhibition Road, London SW7 2BT, UK

(Received 1 September 2011; revised manuscript received 12 January 2012; published 30 April 2012)

A theory is presented combining effective-medium theory with that of magnetoinductive (MI) waves propagating by virtue of coupling between the resonant elements. The resulting circuit equations for the split-ring resonator (SRR) loaded transmission line are shown to be analogous to those describing a continuous anisotropic magnetic plasma exhibiting spatial dispersion due to interelement coupling. Interelement coupling is also shown to govern the properties of both bulk and surface *magnetoinductive polaritons* (hybrid polaritonic modes of electromagnetic waves and of slow waves of coupling between resonators). Implications of our method in the design of structures with controllable effective material parameters and with required functionality are demonstrated. We are able to design SRR-based near field manipulating devices for transverse electric (TE) polarization, including a realization of Pendry's near-perfect lens. Considering that surface waves of various kinds have found a wide range of applications in the past, it is envisaged that surface magnetoinductive polaritons will open up fresh possibilities.

DOI: 10.1103/PhysRevB.85.155146 PACS number(s): 41.20.Jb, 42.25.Bs, 42.70.Qs, 73.20.Mf

I. INTRODUCTION

Born at the turn of the millennium, the subject of metamaterials rapidly evolved into a main stream in physics and engineering. The upsurge of interest originated from a diversity of research directions that fed the young subject, all with the same goal: to be able to assemble structures with desired electromagnetic properties not found in naturally available materials. The approaches to how to look at metamaterials range from effective medium theory to plasma physics and circuit theory.

Effective medium theory has a long history. We still teach in undergraduate courses the Clausius-Mossotti equations derived in the 19th century. The theory is concerned with the introduction of effective material parameters like permeability and permittivity. Having obtained those parameters we can, for most purposes, ignore the microscopic properties of atoms and molecules. This quite simple theory turned out to be one of the most enduring ones in solid state physics: the principles being still applicable when the parameters take negative values as well. See, for example, the papers of Thompson[1] and Pendry *et al.*[2] on negative permeability or that of Rotman[3] on negative permittivity. With the advent of metamaterials, many more papers followed making further advances in the theory (see, e. g., Ref. 4).

Surface waves have been known since about the beginning of the 20th century under names like Sommerfeld,[5] Zenneck,[6] Goubeau[7] waves, and the whole family of surface plasma waves, which are called nowadays surface plasmon polaritons [see, e. g., Refs. 8–10]. Quite obviously, general anisotropic plasma, with either permittivity or permeability being a tensor rather than a scalar, offers a larger degree of freedom for the existence of surface waves. Surface waves in anisotropic dielectrics and magnetic plasmas were described in Ref. 11. In the metamaterial context, surface waves have been found experimentally on a stack of split-ring resonators (SRR) by Gollub *et al.*[12] who referred to them as magnetic surface plasmons and explained them theoretically by assuming an isotropic negative permeability.

Another line of thought also goes back a long time. It is to derive and explain the properties of certain waves by invoking the interaction between elements. The elements may be atoms and molecules, the interaction between them may be restricted to nearest neighbors. From these assumptions, the theory was born of acoustic waves extended later to the optical branch (see Ref. 13). The elements could, of course, be macroscopic ones, e.g., various circuits or resonant structures. Using then the same kind of assumptions about the interaction between the elements, it was possible to explain the propagation of waves in slow wave structures by Silin and Sazonov,[14] in frequency filters by Atabekov,[15] in coupled optical resonators by Yariv *et al.*[16] For an extension of the work to interaction between many (or infinite number) elements see, for example, the paper by Weber and Ford.[17] In the metamaterial context it was shown by Shamonina *et al.*[18,19] that magnetic coupling between elements leads to waves, which have been known since as magnetoinductive or MI waves. When the coupling is electric analogous waves were shown to exist by Baena *et al.*[20] called electroinductive or EI waves. Waves on magnetically coupled elements have also been referred to more recently as magnetization waves[21] and magnetic plasmons.[22] Waves due to interelement coupling are eigenmodes of the metamaterial and, like any eigenmodes of a medium, they can be expected to couple to and influence the propagation of electromagnetic (EM) waves forming hybrid polaritonic modes with electromagnetic waves. A 1D theory incorporating interelement coupling into the effective-medium model was derived by Syms *et al.*.[23] An extension to an isotropic 3D case was devised by Baena *et al.*[24] followed by a further extension by Silveirinha *et al.*[25] that included retardation effects as well.

The present paper combines effective medium theory with interelement coupling in an anisotropic 2D configuration. Hence, following faithfully the traditions of solid-state physics, we shall use the term *magnetoinductive (MI) polaritons*,[26,27] in analogy to plasmon polaritons in a bulk metal or phonon polaritons in a diatomic semiconductor.

We are restricting here the analysis to magnetically coupled elements but of course very similar effects can be expected when the coupling is electric or indeed when it is a combination of magnetic and electric coupling.[28] Starting with a circuit model, we proceed to a description of both the micro and macrophysics, and offer, in addition, a recipe for the design of specific structures. We establish relationships between effective-medium parameters and circuit characteristics of a generally anisotropic 2D metamaterial comprising split rings, unravel the properties of magnetoinductive polaritons both in their bulk and surface variety, and show that the latter can lead to an alternative realization of a superlens.[29] The structure of the paper is as follows. In Sec. II, a transmission-line model is developed describing propagation of electromagnetic waves through a general split-ring structure resulting in a set of difference equations involving the circuit parameters of both electromagnetic and magnetoinductive waves. In Sec. III, the analogy between this discrete circuit model and Maxwell's equations for a transverse electric (TE) wave are discussed yielding effective values of the permeability tensor and in Sec. IV the properties of bulk MI polaritons and conditions for their excitation are described. Analysis in Sec. V valid for semi-infinite media, addresses the question under what conditions these new type of waves have, besides the bulk, a surface wave variety as well. Section VI is a straightforward generalization of the analysis to that of a slab. We systematize conditions for subwavelength imaging, identifying split-ring configurations suitable (as well as those not suitable) for subwavelength imaging via surface modes. Using realistic parameters, we show how the transfer function of a split-ring slab depends on the unit cell size and slab thickness. Finally, we discuss possibilities of generalization of the model to an arbitrary metamaterial structure with interelement coupling. Conclusions are drawn in Sec. VII.

II. CIRCUIT MODEL

We consider a rectangular array of split-ring resonators (SRRs) as shown in Fig. 1(a). It is a generalization of the 1D model of Syms *et al.*[23] to 2D. It consists of two interlaced sublattices, known as planar-axial structures[4] on account of the coupling coefficients being significant both in the planar and in the axial directions. The equivalent circuits of the SRRs in the two sublattices are represented by identical inductance-capacitance (LC) resonators in Fig. 1(b). Taking only nearest neighbors into account, the mutual inductances standing for axial coupling are denoted by the subscript a and those representing planar coupling by the subscript p. The coupling may take place either in the x or in the z directions. Accordingly, as shown in Fig. 1(b), we distinguish four different mutual inductances, M_{ax}, M_{az}, M_{px}, and M_{pz}. It should be noted that another kind of coupling between nearest neighbors in the x and z directions in the same unit cell may also exist. However, we shall disregard them in the present treatment. In an example given in the next section, we shall show that in the structure chosen this type of coupling is entirely negligible.

The electromagnetic wave, with which the split rings interact, is assumed in the form of a TE wave propagating in the xz plane with the electric field in the y direction. Its

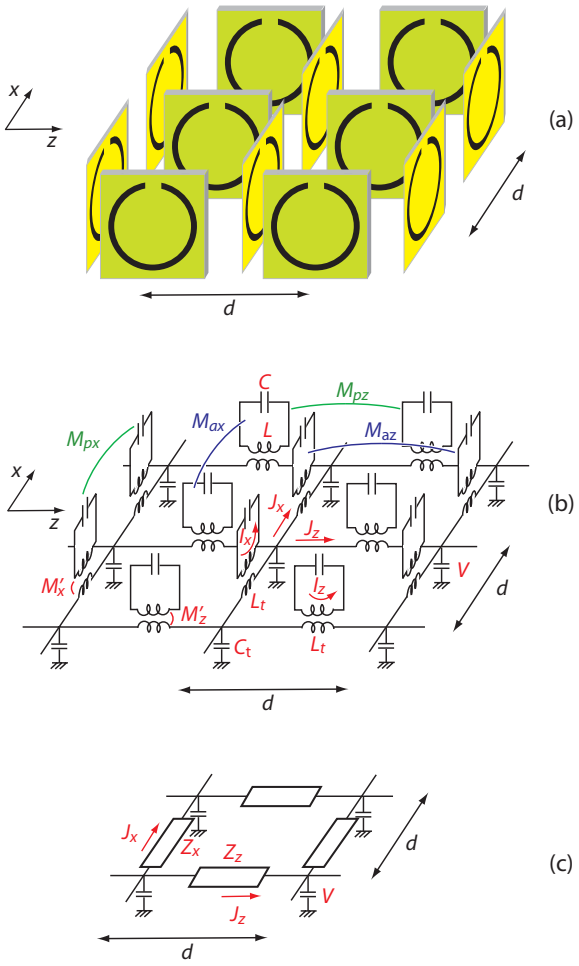

FIG. 1. (Color online) (a) 2D split-ring metamaterial. (b) Its circuit model capable of describing both MI waves and TE electromagnetic waves. (c) The equivalent impedance scheme.

circuit equivalent is the 2D transmission line consisting of an inductance L_t and a capacitance C_t as may also be seen in Fig. 1(b). $L_t = \mu_0 d$ and $C_t = \varepsilon_0 d$, with μ_0 and ε_0 being the permeability and permittivity of vacuum, and d being the unit cell size in both the x and the z directions. To account for the interaction between the electromagnetic wave and the split rings, the elements of this discrete transmission line are coupled to the corresponding resonant circuits by mutual inductances M'_x and M'_z in the two different directions. When the resonant circuits loading the transmission line are independent of each other, then what we have is the traditional model for finding the effective permeability of a SRR metamaterial. Our aim is, however, to combine the effective medium model with the one permitting wave propagation via coupling between the resonant circuits.

Our mathematical treatment starts with the presentation of Kirchhoff's equations. For the voltages, they take the form

$$V_{l+1,m} - V_{l,m} = -\mathrm{j}\omega L_t I_{x,l,m} - \mathrm{j}\omega M'_x J_{x,l,m}, \qquad (1)$$

$$V_{l,m+1} - V_{l,m} = -\mathrm{j}\omega L_t I_{z,l,m} - \mathrm{j}\omega M'_z J_{z,l,m}, \qquad (2)$$

and for the currents,

$$I_{x,l-1,m} + I_{z,l,m-1} = I_{x,l,m} + I_{z,l,m} + \mathrm{j}\omega C_t V_{l,m}, \qquad (3)$$

where $V_{l,m}$ is the voltage across the capacitor between the node l,m and earth, ω is the frequency, $I_{x(z),l,m}$ and $J_{x(z),l,m}$ are the currents flowing in the transmission line and in the resonator in the $x(z)$ direction, respectively. Time variation is assumed in the form $\exp(\mathrm{j}\omega t)$.

Next, we write Kirchhoff's voltage equation for the resonant circuits in the x and z sublattices as

$$Z J_{x,l,m} + \mathrm{j}\omega M'_x I_{x,l,m} + \mathrm{j}\omega M_{\mathrm{px}}(J_{x,l-1,m} + J_{x,l+1,m}) + \mathrm{j}\omega M_{\mathrm{az}}(J_{x,l,m-1} + J_{x,l,m+1}) = 0 \quad (4)$$

and

$$Z J_{z,l,m} + \mathrm{j}\omega M'_z I_{z,l,m} + \mathrm{j}\omega M_{\mathrm{ax}}(J_{z,l-1,m} + J_{z,l+1,m}) + \mathrm{j}\omega M_{\mathrm{pz}}(J_{z,l,m-1} + J_{z,l,m+1}) = 0, \quad (5)$$

where Z is the impedance of the resonant circuit. Note that Eqs. (1)–(5) completely specify the problem. We can express J_x with the aid of I_x from Eq. (4) and substitute it into Eq. (1). Similarly, we can express J_z with the aid of I_z from Eq. (5) and substitute it into Eq. (2). Using further the wave assumption for all the currents and the voltage that they vary along the x and z directions as $\exp[-\mathrm{j}(lk_x d + mk_z d)]$, we obtain

$$V_{l+1,m} - V_{l,m} = -Z_x I_{x,l,m} \quad (6)$$

and

$$V_{l,m+1} - V_{l,m} = -Z_z I_{z,l,m}, \quad (7)$$

where

$$Z_{x(z)} = \mathrm{j}\omega L_{\mathrm{t}}\left(1 - \frac{q^2_{x(z)}}{D_{x(z)}}\right), \quad (8)$$

$$D_{x(z)} = 1 - \frac{\omega_0^2}{\omega^2} + \kappa_{\mathrm{az}(x)}\cos(k_{z(x)}d) + \kappa_{\mathrm{px}(z)}\cos(k_{x(z)}d), \quad (9)$$

with the resonant frequency, $\omega_0 = 1/\sqrt{LC}$, the MI coupling coefficients,

$$\kappa_{\mathrm{a(p)}\,x(z)} = \frac{2M_{\mathrm{a(p)}\,x(z)}}{L}, \quad (10)$$

and the EM-SRR coupling coefficients,

$$q_{x(z)} = \frac{M'_{x(z)}}{\sqrt{LL_{\mathrm{t}}}}, \quad (11)$$

also known as the fill factors, corresponding to the ratio of the SRR area to the area of the unit cell.[4]

Note that expressions (9) for D_x and D_z represent the dispersion equations of the magnetoinductive waves for the two sublattices.[4] Equations (6) and (7) together with Eq. (3) offer the simplified equivalent circuit shown in Fig. 1(c). We now have single equivalent impedances in the x and z directions although, of course, they have a complicated dependence on the parameters as may be seen from Eqs. (8)–(11).

III. EFFECTIVE PERMEABILITY TENSOR IN TERMS OF CIRCUIT QUANTITIES

Our aim in this section is to relate the theory derived so far to that of effective medium theory, i.e., we intend to find the corresponding permeabilities. We shall assume a TE wave when the components of the electric and magnetic fields are E_y, H_x, and H_z and we shall take the diagonal elements of the permeability tensor as μ_x, 1, μ_z. Maxwell's equations for this case may be written as

$$\frac{\partial H_x}{\partial z} - \frac{\partial H_z}{\partial x} = \mathrm{j}\omega\varepsilon_0 E_y,$$
$$\frac{\partial E_y}{\partial z} = \mathrm{j}\omega\mu_0(H_x + M_x) = \mathrm{j}\omega\mu_0\mu_x H_x,$$
$$\frac{\partial E_y}{\partial x} = -\mathrm{j}\omega\mu_0(H_z + M_z) = -\mathrm{j}\omega\mu_0\mu_z H_z, \quad (12)$$

where M_x and M_z are the components of the magnetization. Considering Eqs. (3), (6), and (7) for the discrete case, using the relationship between the discrete and continuous quantities as

$$V_{l,m} = E_y d, \quad I_{x,l,m} = H_z d, \quad I_{z,l,m} = -H_x d \quad (13)$$

and identifying, as mentioned before, C_{t} with $\varepsilon_0 d$, and L_{t} with $\mu_0 d$, we can deduce the equivalent permeabilities as

$$\mu_x = \frac{Z_z}{\mathrm{j}\omega\mu_0 d} \quad \text{and} \quad \mu_z = \frac{Z_x}{\mathrm{j}\omega\mu_0 d}, \quad (14)$$

or, using Eq. (8), as

$$\mu_x = 1 - \frac{q_z^2}{D_z} \quad \text{and} \quad \mu_z = 1 - \frac{q_x^2}{D_x}. \quad (15)$$

In the absence of magnetoinductive coupling (taking all kappas as zero) and with isotropic EM-SRR coupling (taking $q_x = q_z = q$), Eq. (15) reduces to the known result provided by the simplified effective-medium theory:

$$\mu_x = \mu_z = 1 - q^2\frac{\omega^2}{\omega^2 - \omega_0^2}. \quad (16)$$

The presence of magnetoinductive coupling in Eq. (15) results in anisotropy and in spatial dispersion of the permeability.[4,23] Also, the frequency range where permeability is negative can be seen to depend on the MI coupling strength; for small values of kd, where the spatial dispersion can be disregarded, the denominators in Eq. (15) can be approximated by

$$D_{x(z)} \simeq 1 - \frac{\omega_0^2}{\omega^2} + \kappa_{\mathrm{az}(x)} + \kappa_{\mathrm{px}(z)}. \quad (17)$$

Depending on the value and on the sign of the coupling constants, the shift can be both positive and negative.

Next, we relate the macroscopic field quantities to the circuit parameters. The relationship between the magnetic fields H_x and H_z and the currents I_z and I_x is already given by Eq. (13), as

$$H_x = -\frac{I_z}{d}, \quad H_z = \frac{I_x}{d}, \quad (18)$$

where

$$I_{x(z)} = \frac{V}{Z_{x(z)}}[1 - \mathrm{e}^{-\mathrm{j}k_{x(z)}d}]. \quad (19)$$

The expressions for the magnetization components, M_x and M_z follow from Eqs. (1)–(3) and (12) as

$$M_x = -\frac{J_z M'_z}{L_{\mathrm{t}} d}, \quad M_z = \frac{J_x M'_x}{L_{\mathrm{t}} d}, \quad (20)$$

where

$$J_{x(z)} = -\frac{q_{x(z)}}{D_{x(z)}}\sqrt{\frac{L_t}{L}}I_{x(z)}. \quad (21)$$

Note that particularly simple results are obtained in the symmetric case (equal fill factors $q_x = q_z$) when there are no MI interactions (all kappas taken as zero).

IV. BULK MAGNETOINDUCTIVE POLARITONS

From Eqs. (3), (6), and (7), we obtain the following dispersion equation

$$Z_x Z_z Y_y + 4Z_x \sin^2\frac{k_z d}{2} + 4Z_z \sin^2\frac{k_x d}{2} = 0 \quad (22)$$

or, in the alternative form,

$$D_x D_z T = q_x^2 D_z F_z + q_z^2 D_x F_x + q_x^2 q_z^2 \frac{\omega^2}{\omega_t^2}, \quad (23)$$

where $\omega_t = 1/\sqrt{L_t C_t}$,

$$T = -\frac{\omega^2}{\omega_t^2} + 4\sin^2\frac{k_z d}{2} + 4\sin^2\frac{k_x d}{2}, \quad (24)$$

$$F_{x(z)} = -\frac{\omega^2}{\omega_t^2} + 4\sin^2\frac{k_{x(z)} d}{2}. \quad (25)$$

Equation (23) may be easily interpreted physically. It describes how the solution for propagating TE electromagnetic wave and the eigenmodes of the metamaterial (MI waves) are transformed to polaritonic states of mixed modes. On the left-hand side, we have the product of three functions: D_x, D_z, and T. If the right-hand side (RHS) is zero, then these functions represent three independent dispersion characteristics: two independent MI waves for the two sublattices of the structure (terms D_x and D_z) and a very familiar wave that propagates on a 2D transmission line consisting of an infinite set of discrete $L_t C_t$ circuits (term T). In the continuous limit ($k_x d, k_z d \ll 1$), the latter corresponds to the electromagnetic wave, taking the simplified form

$$T = \left(-\frac{\omega^2}{c^2} + k_z^2 + k_x^2\right)d^2. \quad (26)$$

The resulting hybrid modes have striking similarities with plasmon polaritons although the physics is different: the characteristics depend on the interaction between neighboring elements. Equation (23) is a cubic in $u = \omega_0^2/\omega^2$ yielding three branches of the dispersion equation. Although the coupling coefficients may be small their influence upon the dispersion characteristics can be significant as shown in the examples below.

For the planar-axial configuration shown in Fig. 2(a), i.e., in the absence of one of the sublattices in Fig. 1, the corresponding dispersion equation reduces to a quadratic one:

$$D_z T = q_z^2 F_x. \quad (27)$$

The resulting dispersion has two branches. If the RHS is zero, they correspond to the unperturbed magnetoinductive wave of the planar-axial array (term D_z) and TE electromagnetic wave (term T). The condition for the RHS to be nonzero is particularly easy to interpret. The coupling between the EM and MI modes is provided via q_z but it occurs only if there is a nonzero k_z component of the EM wave. This means physically that a nonzero H_x component is needed for the excitation of the planar-axial array considering that the SRRs lie in the yz plane.

We will illustrate the properties of bulk magnetoinductive polaritons on a number of examples including the planar-axial structure [see Fig. 2(a)], the symmetric structure [see Fig. 2(b)] and the "brick wall" [see Fig. 2(d)]. The inclusion of the last one needs some explanation. Our aim is to arrive at a simple structure in which coupling in the x direction is eliminated to a good approximation. The first step toward this elimination is the structure of Fig. 2(c) in which the sublattice of "horizontal" elements is shifted by half a period in the vertical, x, direction relative to the structure of Fig. 2(b). There is now clearly no interaction between the "vertical" and "horizontal" elements in the same row justifying our earlier assumption that this type of coupling can be neglected. We can further reduce or eliminate coupling between certain pair of elements by shifting every second row in the horizontal direction arriving at the structure shown in Fig. 2(d), which for obvious reasons we call the brick-wall structure.

In the brick-wall structure, there is no interaction between vertical and horizontal neighbors within each column [see Fig. 3(a)] and within each row [see Fig. 3(b)]. Furthermore, by judicious design, the coupling between both vertical [see Fig. 3(c)] and horizontal [see Fig. 3(d)] elements in neighboring rows can be eliminated.[30] There will of course be interactions between elements (both vertical and horizontal) two rows or two columns away from each other but those will be much weaker so in first-order approximation they can be neglected [seee Figs. 3(e)–3(h)]. Hence, for the brick-wall structure, it is sufficient to take into account interactions only between neighboring elements within each row as indicated by arrows in Fig. 2(d).

Figures 4–6 show dispersion curves [see Eqs. (27) and (23)] as 3D surfaces $\omega(k_x, k_z)$ for the planar-axial, the symmetric and the brick-wall structures, respectively. Figures 7–9 show

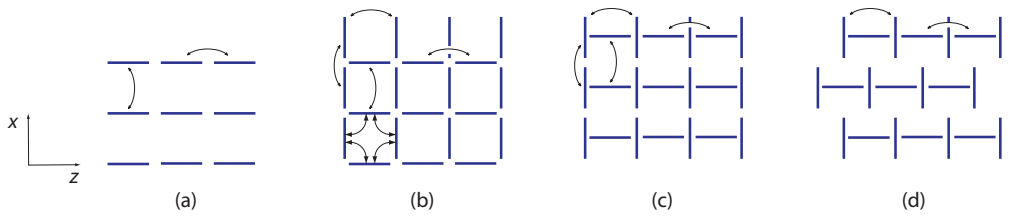

FIG. 2. (Color online) Side view of the SRRs. Wave propagation in the z direction. (a) Planar-axial structure. (b)–(d) Tailoring the coupling: transition from two coupled sublattices of SRRs (b) to two uncoupled sublattices of SRRs (c) and to the brick-wall structure with coupling only in the z direction (d). The dominant coupling coefficients are shown by black arrows.

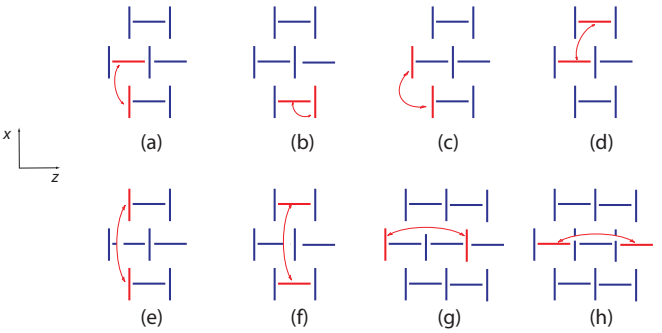

FIG. 3. (Color online) Elimination of coupling between elements shown in red in the brick-wall structure.

the corresponding dispersion curves plotted along the paths ΓXMΓ and ΓZMΓ of the 1st Brillouin zone. Note that the value of ω_t/ω_0 in these examples was chosen to be very small, equal to 1.6, in order to show more clearly the range of the interaction (this value corresponds to the resonant frequency $\omega_0/2\pi = 100$ MHz and a unit cell size of $d = \lambda/10$). In each of the cases, we switch on and off EM-SRR coupling and MI coupling, which, when not switched off, are taken as (1) $q_z^2 = 0.2$, $\kappa_{ax} = 0.1$, $\kappa_{pz} = -0.1$ (Fig. 4, planar-axial), (2) $q_z^2 = q_x^2 = 0.2$, $\kappa_{ax} = \kappa_{az} = -\kappa_{px} = -\kappa_{pz} = 0.1$ (Fig. 5, symmetric), and (3) $q_z^2 = q_x^2 = 0.2$, $\kappa_{az} = -\kappa_{px} = 0.1$, $\kappa_{ax} = \kappa_{pz} = 0$ (Fig. 6, brick wall).

For circularly shaped split rings, the values of 0.1 and −0.1 for magnetoinductive coupling coefficients kappas correspond to the center-to-center distance approximately equal to the diameter of the rings in the axial and in the planar arrangement, respectively, whereas the value of 0.2 for the fill factor (representing the ratio of the SRR area to the area of the unit cell) is close to a typical value of 0.4 often quoted in the literature.[4]

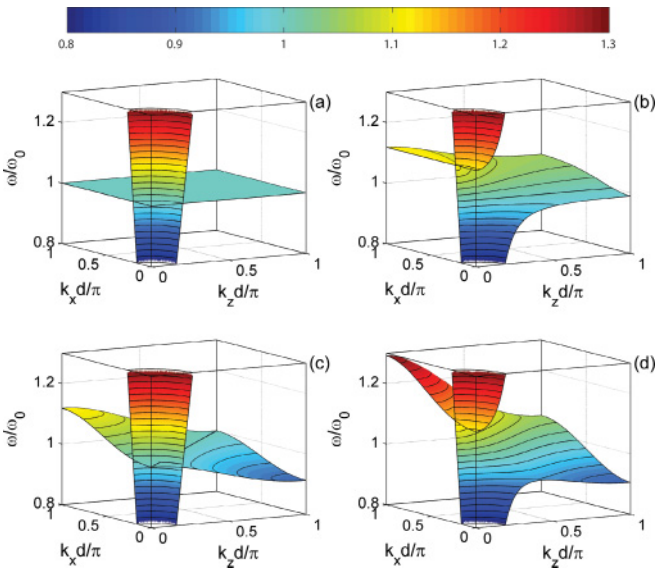

FIG. 4. (Color online) Planar-axial structure of Fig. 2(a). Dispersion of bulk MI polaritons. (a) Unperturbed case, no EM-SRR coupling, no MI coupling. (b) With EM-SRR, but without MI coupling. (c) Without EM-SRR coupling, but with MI coupling; (d) with both EM-SRR and MI coupling. Color bar corresponds to the values of ω/ω_0.

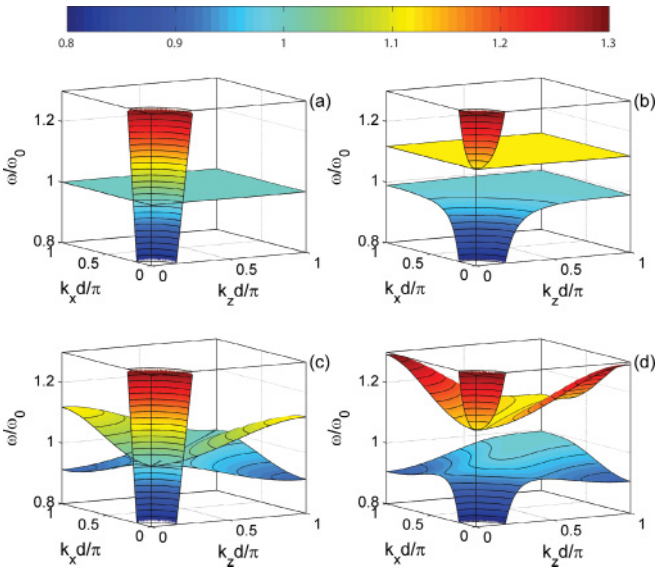

FIG. 5. (Color online) Symmetric structure of Fig. 2(b) without coupling between horizontal and vertical sublattices. (a)–(d) Dispersion of bulk MI polaritons. (a) Unperturbed case, no EM-SRR coupling, no MI coupling. (b) With EM-SRR, but without MI coupling. (c) Without EM-SRR coupling, but with MI coupling; (d) with both EM-SRR and MI coupling. Color bar corresponds to the values of ω/ω_0.

As expected, the planar-axial case (see Fig. 4) exhibits only two branches of bulk magnetoinductive polaritons, whereas the symmetric (see Fig. 5) and the brick-wall (see Fig. 6) cases have three branches each. It can be seen that plots (a) are identical in all configurations. In this trivial case of no EM-SRR and MI coupling, the branches are the unperturbed electromagnetic wave (seen as a light cone) and

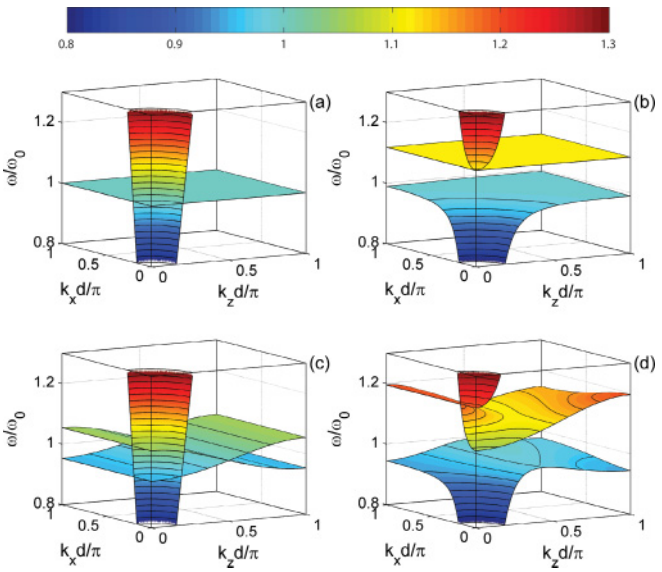

FIG. 6. (Color online) Brick-wall structure of Fig. 2(d). (a)–(d) Dispersion of bulk MI polaritons. (a) Unperturbed case, no EM-SRR coupling, no MI coupling. (b) With EM-SRR, but without MI coupling. (c) Without EM-SRR coupling, but with MI coupling; (d) with both EM-SRR and MI coupling. Color bar corresponds to the values of ω/ω_0.

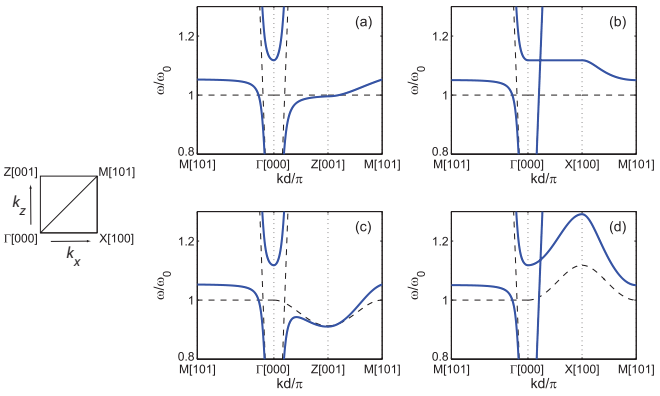

FIG. 7. (Color online) Planar-axial structure of Fig. 2(a). Dispersion of bulk MI polaritons along the ΓZMΓ path (left column) and ΓXMΓ path (right column). Dashed lines: no EM-SRR coupling. Solid lines: with EM-SRR coupling. Top row: no MI coupling. Bottom row: with MI coupling.

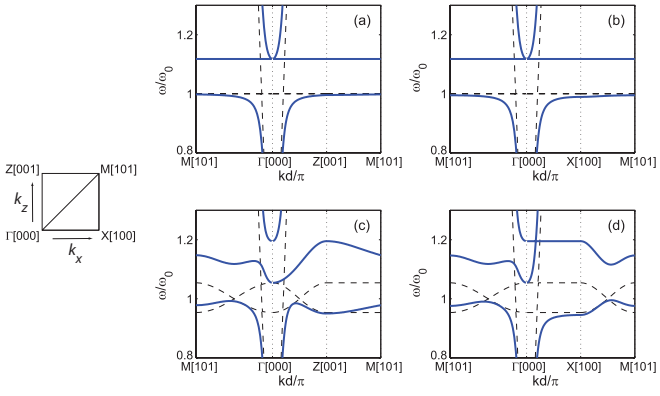

FIG. 9. (Color online) Brick-wall structure of Fig. 2(d). Dispersion of bulk MI polaritons along the ΓZMΓ path (left column) and ΓXMΓ path (right column). Dashed lines: no EM-SRR coupling. Solid lines: with EM-SRR coupling. Top row: no MI coupling. Bottom row: with MI coupling.

the eigenmodes of the metamaterial in this case simply given by the single resonance frequency of the split rings (horizontal plane $\omega = \omega_0$). In case (b), in the absence of magnetoinductive coupling, Eqs. (23) and (27) reduce to the known result provided by the simplified effective-medium theory describing the propagation of a TE wave in a SRR medium. Both Figs. 5(b) and 6(b) coincide giving three branches exhibiting identical behavior in the x and z directions. This could be expected due the equal number of SRRs oriented in the xy and in the zy planes. The resulting polaritonic states of mixed modes have simple properties. A stop band for bulk modes appears due to the range of negative permeability. In case (c)—no interaction with EM waves—we can see the unperturbed light cone together with unperturbed 2D dispersions of MI waves. In all three configurations, the corresponding dispersions look different. The MI dispersion for the planar-axial configuration [see Fig. 4(c)] shows a backward wave character along the z and a forward wave character along the x axis. The symmetric configuration [see Fig. 5(c)] consisting of two identical planar-axial sublattices mirrored relative to the axis $x = z$ unsurprisingly shows two identical branches of MI waves, also mirrored relative to the $k_x = k_z$ axis. This is because in the symmetric configuration of Fig. 2(b) the coupling coefficients are fully symmetric, there is an obvious fourfold symmetry as the x and z directions are interchangeable. The brick-wall configuration [see Fig. 6(c)] shows two branches of two sublattices with MI coupling only in the z direction, and as a result, both being independent of k_x. One sublattice carries a forward MI wave and the other one a backward MI wave along the z direction. Case (d) looks of course different but not drastically different. With a bit of imagination their origin in cases (b) and (c) could be recognized. Interestingly, for the planar-axial configuration [see Fig. 4(d)] the two branches remain uncoupled for propagation in the x direction ($k_z = 0$). This is not surprising, considering that the SRRs being oriented in the yz plane need a nonzero H_x component to be excited and this is missing in the TE mode having k_x vector only.

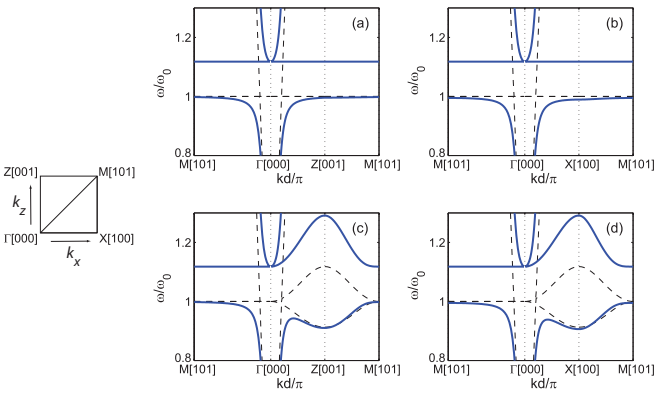

FIG. 8. (Color online) Symmetric structure of Fig. 2(b) without coupling between the horizontal and the vertical sublattices. Dispersion of bulk MI polaritons along the ΓZMΓ path (left column) and ΓXMΓ path (right column). Dashed lines: no EM-SRR coupling. Solid lines: with EM-SRR coupling. Top row: no MI coupling. Bottom row: with MI coupling.

The way to look at and appreciate dispersion characteristics depends largely on one's previous experience. One way of looking at them has been given by Figs. 4–6. We believe however that much would be gained if we added to this another representation [see Figs. 7–9] favored by solid state physicists. Note that the Z direction (see left column) corresponds to k_z and the X direction (right column) to k_x when compared with our previous notations. There are still four subplots for each figure but in a different arrangement. The absence of EM coupling is now shown by dashed lines in all four subplots. Panels (a) and (b) show the dispersion curves in the absence and panels (c) and (d) in the presence of MI coupling. There is, of course, no new information given in Figs. 7–9 relative to Figs. 4–6. However, some of the information is presented in a more quantitative and therefore more digestible form. For example, the effect of EM interaction is much better indicated and in particular it is now much clearer [see, e.g., Fig. 7(b)] that dispersion characteristics can cross each other without any interaction. The reason can be found in the polarizations of those waves.

A major advantage of our approach is that we have analytical expressions for the field quantities enabling us to plot not only the dispersion curves but also the polarization properties. As may be expected, the polarizations will, in general, be

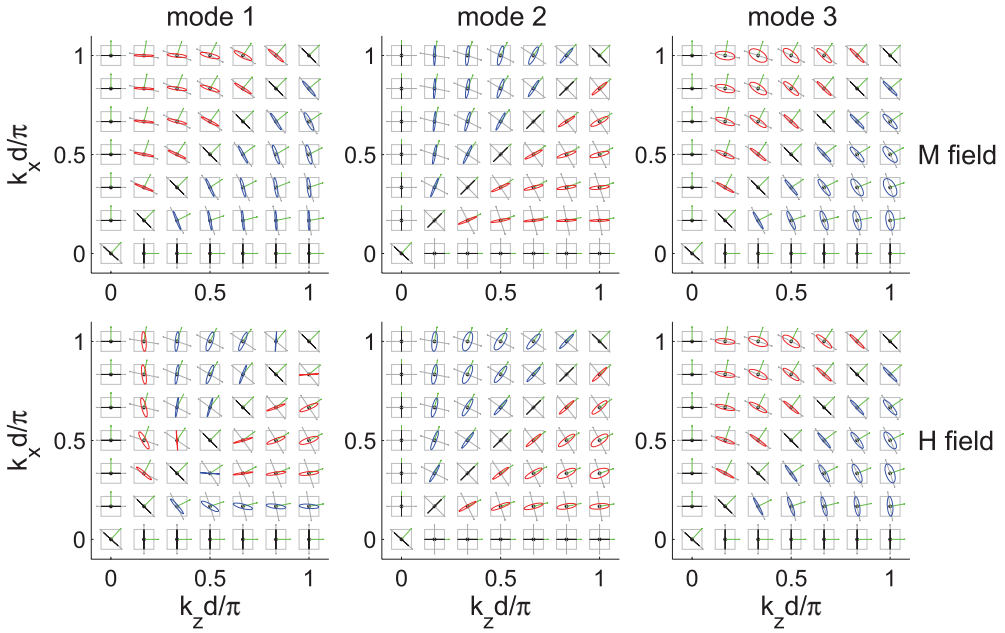

FIG. 10. (Color online) Polarization ellipses for the symmetric configuration of Fig. 2(b) plotted at regular intervals in the k_x-k_z plane for the three branches of the dispersion surfaces. First row is the magnetization, second row is the magnetic field.

elliptical. Figure 10 shows, for the symmetric configuration of Fig. 2(b), the polarization ellipses of M and H, at selected points in the 1st Brillouin zone. The three branches are numbered as 1, 2, 3 with ascending frequency. The polarization state is shown by ellipses (right-elliptical polarization in red, left-elliptical in blue, and linear polarization in black). Also shown, as green lines, the direction of the wave vector in each of the points of the Brillouin zone, and, as grey lines, the direction perpendicular to the wave vector.

It can be seen that, for propagation along either the x axis, the z axis or the diagonal $x = z$ the 1st and the 3rd modes are purely transverse, whereas the 2nd mode is purely longitudinal. This is in agreement with the result by Baena *et al.*.[24] However, the polarization becomes increasingly elliptical for other propagation directions. In particular, for the 2nd mode, the presence of nonlongitudinal polarization shows the presence of coupling between EM and MI wave.

The argument supporting this statement is analogous to that often used in plasma physics. The dispersion equation (23) is, for the continuous case, equivalent to

$$\mathrm{div}\mathbf{B} = \mathrm{div}(\mu\mathbf{H}) = \mathbf{0}. \tag{28}$$

In the simplest case of no MI coupling and for $q_x = q_z$, we deal with the isotropic case of $\mu_x = \mu_z$. Then, there are two possibilities to satisfy Eq. (28), either if

$$\mathrm{div}\mathbf{H} = \mathbf{k}\cdot\mathbf{H} = \mathbf{0}, \tag{29}$$

yielding the transverse mode with $\mathbf{k}$ perpendicular to $\mathbf{H}$ or if

$$\mu = 0, \tag{30}$$

for which we are left with the option that the wave is longitudinal. In case of anisotropic permeability tensor, the argument is no longer valid. Considering the symmetric configuration of Fig. 2(b), similar analysis leads to the conclusion that the 2nd mode is longitudinal only for the symmetry axes x, z and $x = z$, otherwise the spatial dispersion and anisotropy of permeability does not permit the existence of purely longitudinal bulk MI polaritons. Therefore we can safely assume that for the majority of practically relevant cases, most bulk modes of MI polaritons will be excited by an incident TE electromagnetic wave. For the brick-wall structure, the ellipticity becomes even more prominent and the pureness of the longitudinal/transverse modes is preserved only for propagation along the crystallographic axes (not shown).

V. SURFACE WAVES: SEMI-INFINITE MEDIA

Surface waves on metamaterials have been reported before by Sanada[31] and Radkovskaya *et al.*[32] but in both cases the surface wave propagated between two judiciously designed metamaterials. The question we are asking here whether a surface wave analogous to a surface plasmon polariton can also exist in any of our structures, i.e., do surface magnetoinductive polaritons exist? With that aim in mind, we shall now look at the conditions under which surface waves can propagate along the boundary of media 1 and 2 (located at $x = 0$) when medium 1 is vacuum occupying the lower half plane and medium 2 is our anisotropic magnetic plasma (abbreviated hence by AMP). If it is a surface wave, the fields must decline away from the boundary. Consequently, the decays in the two media are assumed in the form $\exp(\kappa_1 x)$ and $\exp(-\kappa_2 x)$ where both κ_1 and κ_2 are assumed to be positive and the subscripts 1 and 2 refer to the respective media. Solving Eq. (12) both in air and in the AMP and noting that the waves must travel along the interface, i.e., in the z direction, at the same velocity in both media, we find the relationship in medium 1 as

$$k_z^2 - \kappa_1^2 = k_0^2 \tag{31}$$

and medium 2 as

$$\mu_z k_z^2 - \mu_x \kappa_2^2 = \mu_x \mu_z k_0^2, \quad k_0 = \frac{\omega}{c}, \tag{32}$$

and we have a further equation, relating κ_2 and κ_1 to each other, by satisfying the boundary conditions at $x = 0$ for the tangential components of the electric and magnetic fields in the form

$$-\kappa_1 \mu_z = \kappa_2, \tag{33}$$

where c is the velocity of light in vacuum. It may be seen from Eq. (33) that a necessary condition is that

$$\mu_z < 0. \tag{34}$$

Further algebraic manipulations yield for the wave number in the z direction,

$$k_z^2 = k_0^2 \frac{\mu_x(1-\mu_z)}{1-\mu_x\mu_z}. \tag{35}$$

For a surface wave to propagate, we need the inequality $k_z > k_0$. This criterion is satisfied when

$$\mu_x > 1 \tag{36}$$

for positive μ_x and when

$$|\mu_x| > |\mu_z|^{-1} \tag{37}$$

for negative μ_x. The dispersion equation can be found by substituting into Eq. (35) the frequency dependence of the two components of permeability given by Eq. (14).

In the planar-axial structure of Fig. 2(b) with SRR normals in the x direction, the z component of the permeability is unity, $\mu_z = 1$. Immediate consequence is that there cannot be any surface MI polaritons propagating along the surface $x = \text{const}$.

The situation is quite different for the brick-wall structure of Fig. 2(d). In Fig. 11, using the same parameters as in Fig. 6(d), we plot dispersion curves for already familiar bulk modes, and, besides, the surface-mode dispersion characteristics as well. For convenience, we also plot five asymptotic lines: $\mu_z = \pm\infty$, $\mu_x = \pm\infty$, $\mu_z = 0$, $\mu_x = 0$, and $\mu_x\mu_z = 1$. The surface mode can be seen to originate at the point where the $\mu_z = \pm\infty$ line intersects the light line $\omega/k_z = c$, and, for large k_z, it asymptotically approaches the $\mu_x\mu_z = 1$ line and can exhibit strong spatial dispersion. Depending on the relative values of the planar and axial coupling coefficients, the surface MI polariton can be a forward or a backward wave. This may be seen in Fig. 12(a) where we show surface-mode dispersion along the surface $x = \text{const}$ for various MI coupling coefficients using the condition $\kappa_a - \kappa_p = 0.2$ and taking $q_x^2 = q_z^2 = 0.2$. It leads to a forward wave when the axial coupling is dominant and to a backward wave when the planar coupling is higher. Returning to the $\kappa_p = -0.1, \kappa_a = 0.1$ case the effect of q^2, the coupling between the electromagnetic wave and the SRRs, is investigated in Fig. 12(b). As may be expected, higher EM-SRR coupling leads to a wider band for surface waves.

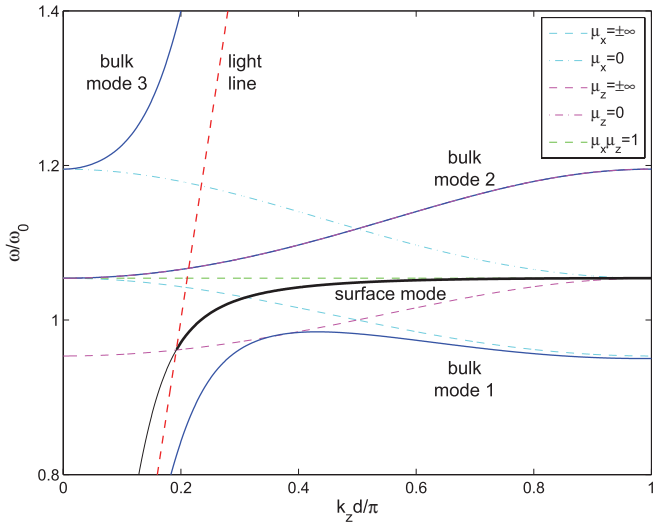

FIG. 11. (Color online) Bulk and surface MI polaritons of the brick-wall structure with an interface air/metamaterial at $x = 0$. Blue lines: bulk modes, black line: surface mode. Also shown asymptotes for permeability and the light line.

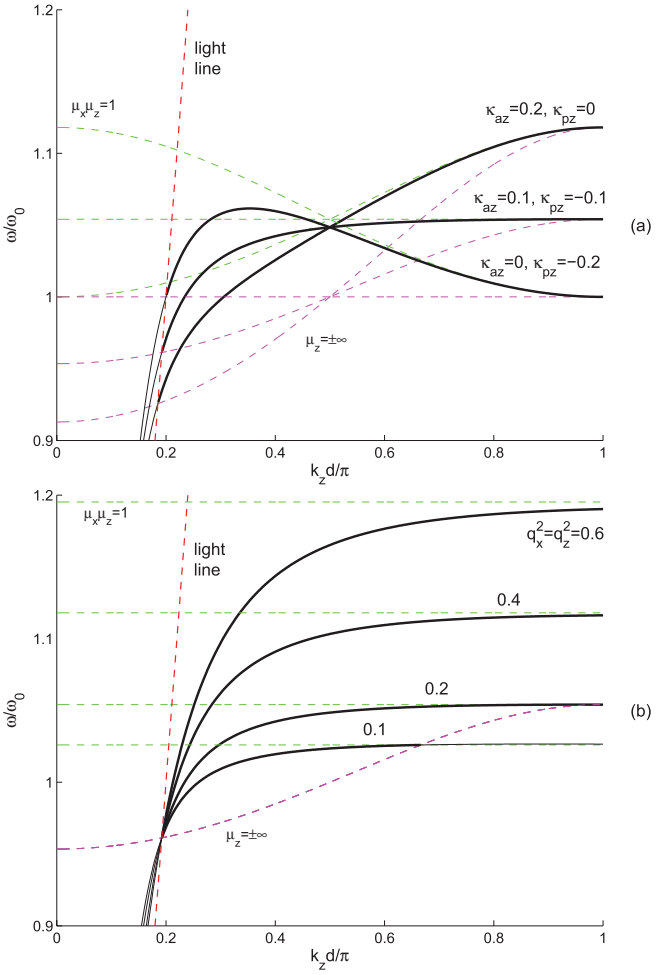

FIG. 12. (Color online) Surface MI polaritons. (a) Effect of MI coupling, (b) effect of EM-SRR coupling.

VI. SPLIT-RING SLAB

This is a straightforward generalization of the treatment in Sec. IV to the case when there are three media: an AMP slab of thickness D surrounded by vacuum on both sides,

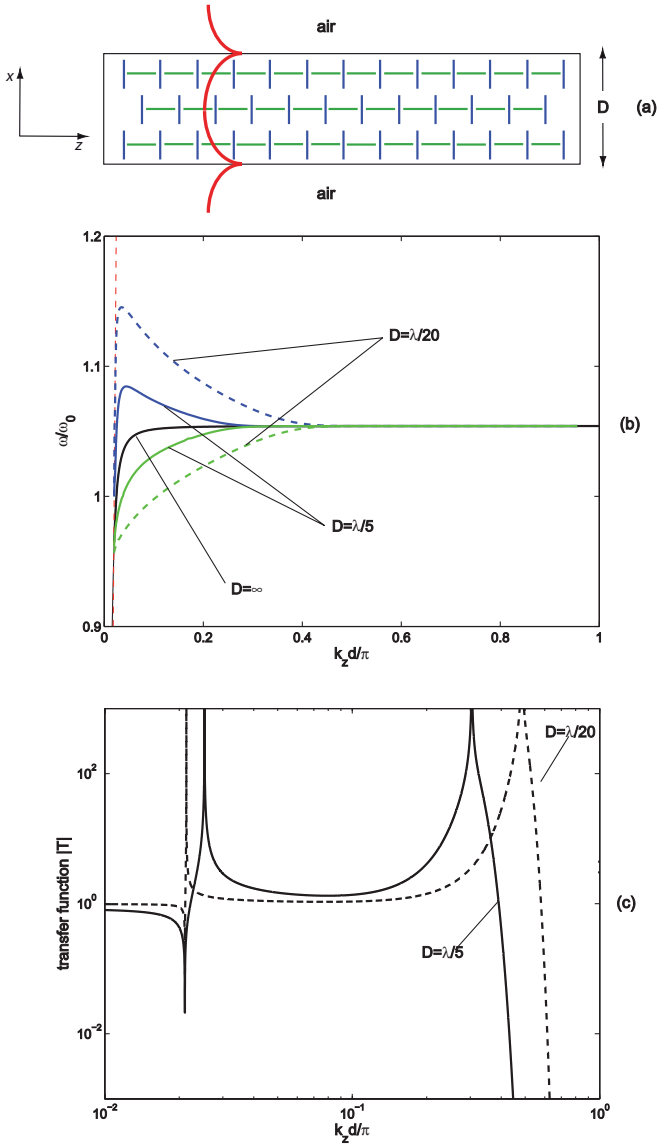

FIG. 13. (Color online) Surface MI polaritons of a slab. (a) Top view of a slab of a brick-wall structure. (b) Surface MI polariton dispersion for various thicknesses D of the brick-wall slab and (c) the corresponding transfer function at the optimum frequency.

see Fig. 13(a). The model is exactly the same as for surface-plasmon slabs: a surface wave propagates in the z direction and the fields decline away in the transverse direction from both surfaces of the slab. The transfer function across the slab for an incident electromagnetic wave with the component along the boundary, can be obtained in the form

$$T = \frac{4\zeta}{(1+\zeta)^2 \exp(\kappa_2 D) + (1-\zeta)^2 \exp(-\kappa_2 D)} \tag{38}$$

with $\zeta = \mu_z \kappa_2 / \kappa_1$. The dispersion equation is obtained from the condition that the denominator in Eq. (38) is zero. Performing the calculations we obtain the following two solutions reminiscent to those for surface plasmons (see, e.g., Ref. 4):

$$\zeta = -\tanh \frac{\kappa_2 D}{2} \quad \text{and} \quad \zeta = -\coth \frac{\kappa_2 D}{2}. \tag{39}$$

To solve the dispersion equation we need again the frequency dependence of μ_x and μ_z from Eq. (15) and, of course, we still need to satisfy Eqs. (31) and (32). Taking as an example a brick-wall structure of thickness D shown in Fig. 13(a) with elements coupled only in the z direction, we obtain dispersion curves for the coupled surface modes shown in Fig. 13(b) with D as a parameter taking values of $\lambda/20$, $\lambda/5$, and ∞. The parameters are the same as in previous brick-wall examples, except that for the unit cell size, we take now a more realistic[4] value of $d = \lambda/100$. The analogy with surface plasmon polaritons on a silver slab can be clearly seen. Not only the forward waves but the backward waves found first by Oliner and Tamir[9] are also present. Figure 13(c) shows the transfer function for the superlens of thickness D, operating at $\omega/\omega_0 = 1.05$, for image transfer from the object plane to the image plane, both being $D/2$ distance away from the boundaries of the slab. It may be seen that for $D = \lambda/5$ the approximately flat region of the transfer function extends up to $k_z d/\pi \simeq 0.2$ and for $D = \lambda/20$ the flat region goes up to $k_z d/\pi \simeq 0.3$. With $d = \lambda/100$ this corresponds to about $k_z/k_0 \simeq 10$ and 15, yielding a resolution of about $\lambda/10$ and $\lambda/15$, respectively, well below the size that can be resolved by classical means.

The conclusions are encouraging. In full analogy to the silver slab, the magnetoinductive polaritonic slab can act as a superlens with resolution improving for thinner slabs. The roughness of such a slab is determined by the unit cell size and manufacturing tolerances (in our example, $d = \lambda/100$ may be expected to provide a sufficiently smooth surface), and the slab thickness determines the resolution—the thinner the slab the better.

VII. CONCLUSIONS

A two-dimensional theory has been developed that combines traditional effective medium theory with the theory of magnetoinductive waves using as a model a metamaterial built up from split-ring resonators. Taking into account nearest-neighbor coupling between the elements, expressions have been derived for the diagonal elements of the permeability tensor. Coupling has been shown to have considerable influence upon the tensor elements. Dispersion characteristics of several configurations have been investigated; the well-known planar-axial and the symmetric structures, to which a new configuration, the brick-wall structure, has been added. It has been shown for the first time that besides bulk waves, a magnetic metamaterial with interelement coupling is capable of propagating surface waves as well. The resulting waves bear strong similarity to surface plasmon polaritons but differ from them in two important aspects: the interaction responsible for their existence is that between individual SRRs and the electromagnetic wave is not a TM but a TE wave. Elliptic polarization states of both the magnetization and of the magnetic field have been calculated analytically demonstrating that in most anisotropic cases the MI polariton is not a pure longitudinal or pure transverse mode. The analogy with surface plasmon polaritons has also been extended to a slab geometry. It has been shown that the brick-wall structure is suitable for the realization of the near-perfect superlens. The basic formulation can be extended to include modifications of the unit cell, and include retardation, losses and higher-order interactions, and,

of course, the same type of phenomena can be expected when the interaction between the elements is electric or a combination of electric and magnetic coupling. Obvious generalizations could be to multilayered and cylindrical superlenses.[4]

ACKNOWLEDGMENT

Financial support of the Leverhulme Trust is gratefully acknowledged.

*ekaterina.shamonina@aot.uni-erlangen.de

[1] G. H. B. Thompson, Nature (London) **175**, 1135 (1955).
[2] J. B. Pendry, A. J. Holden, D. J. Robbins, and W. J. Stewart, IEEE Trans. Microw. Theor. Tech. **47**, 2075 (1999).
[3] W. Rotman, IRE Trans. Ant. Prop. **10**, 82 (1962).
[4] L. Solymar and E. Shamonina, *Waves in Metamaterials* (Oxford University Press, Oxford, 2009).
[5] A. Sommerfeld, Ann. Phys. Chem. **303**, 233 (1909).
[6] J. Zenneck, Ann. Phys. (Leipzig) **23**, 846 (1907).
[7] G. Goubeau, J. Appl. Phys. **21**, 1119 (1950).
[8] U. Fano, J. Opt. Soc. Am. **31**, 213 (1941).
[9] A. A. Oliner and T. Tamir, J. Appl. Phys. **33**, 231 (1962).
[10] S. Maier, *Plasmonics: Fundamentals and Applications* (Springer, Berlin, 2007).
[11] N. Ilin, A. Smirnov, and I. Kondratiev, Metamaterials **3**, 82 (2009).
[12] J. N. Gollub, D. R. Smith, D. C. Vier, T. Perram, and J. J. Mock, Phys. Rev. B **71**, 195402 (2005).
[13] L. Brillouin, *Wave Propagation in Periodic Structures* (Dover, New York, 1953).
[14] R. A. Silin and V. P. Sazonov, *Slow Wave Structures* (Sovetskoe Radio, Moscow, 1966).
[15] G. I. Atabekov, *Linear Network Theory* (Pergamon Press, Oxford, 1965).
[16] A. Yariv, Y. Xu, R. K. Lee, and A. Scherer, Opt. Lett. **24**, 711 (1999).
[17] W. H. Weber and G. W. Ford, Phys. Rev. B **70**, 125429 (2004).
[18] E. Shamonina, V. A. Kalinin, K. H. Ringhofer, and L. Solymar, Electron. Lett. **38**, 371 (2002).
[19] E. Shamonina, V. A. Kalinin, K. H. Ringhofer, and L. Solymar, J. Appl. Phys. **92**, 6252 (2002).
[20] J. D. Baena, J. Bonache, F. Martin, R. Marques, F. Falcone, T. Lopetegi, M. A. G. Laso, J. Garcia-Garcia, M. F. Portillo, and M. Sorolla, IEEE Trans. MTT **53**, 1451 (2005).
[21] G. Dolling, M. Wegener, A. Schädle, S. Burger, and S. Linden, Appl. Phys. Lett. **89**, 231118 (2006).
[22] H. Liu, D. A. Genov, D. M. Wu, Y. M. Liu, J. M. Steele, C. Sun, S. N. Zhu, and X. Zhang, Phys. Rev. Lett. **97**, 243902 (2006).
[23] R. R. A. Syms, E. Shamonina, V. Kalinin, and L. Solymar, J. Appl. Phys. **97**, 064909 (2005).
[24] J. D. Baena, L. Jelinek, R. Marques, and M. Silveirinha, Phys. Rev. A **78**, 013842 (2008).
[25] M. G. Silveirinha, J. D. Baena, L. Jelinek, and R. Marques, Metamaterials **3**, 115 (2009).
[26] E. Shamonina and A. Radkovskaya, in *Proceedings of the Forth International Congress on Advanced Electromagnetic Materials in Microwaves and Optics: Metamaterials 2010*, ISBN 978-952-7734-6 (Karlsruhe, 2010).
[27] E. Shamonina, in *Proceedings of the Fifth International Congress on Advanced Electromagnetic Materials in Microwaves and Optics: Metamaterials 2011*, ISBN 978-952-67611-0-7 (Barcelona, 2011).
[28] E. Tatartschuk, N. Gneiding, F. Hesmer, A. Radkovskaya, and E. Shamonina (unpublished).
[29] J. B. Pendry, Phys. Rev. Lett. **85**, 3966 (2000).
[30] O. Sydoruk, A. Radkovskaya, O. Zhuromskyy, E. Shamonina, M. Shamonin, C. J. Stevens, G. Faulkner, D. J. Edwards, and L. Solymar, Phys. Rev. B **73**, 224406 (2006).
[31] A. Sanada, C. Caloz, and T. Itoh, IEEE MTT-S Int. Microw. Symposium Digest (2005).
[32] A. Radkovskaya, E. Tatartschuk, O. Sydoruk, E. Shamonina, C. J. Stevens, D. J. Edwards, and L. Solymar, Phys. Rev. B **82**, 045430 (2010).